Deterministic trapping, encapsulation and retrieval of single-cells

M. Sauzade and **E. Brouzes**[a]

[a]Department of Biomedical Engineering, Stony Brook University, Stony Brook, NY 11794-5281

Abstract

We present a novel method for conducting true single-cell encapsulation at very high efficiency for the manipulation of precious samples. Our unique strategy is based on the sequential capture and original encapsulation of single-cells into a series of hydrodynamic traps. We identified two distinct modes of encapsulation and we established their associated design rules. We improved the trapping scheme to reach a near perfect capture efficiency and make it compatible with the encapsulation process. Finally, we developed the complete device operation that permits highly efficient single-cell encapsulation and droplet retrieval. This platform provides the foundation to a fully integrated multiparameter platform that will impact the analysis of tissues at single-cell resolution.

Table of content entry
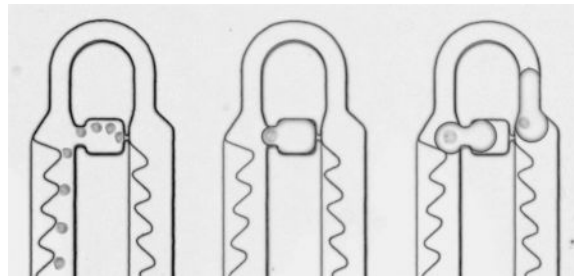
Passive strategy for efficient true single-cell encapsulation.

Introduction

Evidence suggests that studying the heterogeneity of cell populations is critical for cancer research, developmental biology, drug screening, and stem cell research.[1–3] Consequently, researchers have investigated gene expressions, protein levels and metabolites at the level of individual cells.[4–8] Recently, microfluidic technologies have complemented traditional methods for single-cell analysis thanks to their multiplexing capabilities, unparalleled experimental control and reduced sample volumes.[9, 10]

Most approaches make use of droplet microfluidics to isolate minute amounts of samples within aqueous droplets surrounded by immiscible oil.[11–14] Droplets serve as micro vessels, confining cell(s), reagents, and any secreted molecules,[15, 16] while allowing sample manipulation without dispersion. The encapsulated cells can then be processed at high-

throughput using modules derived from a well-established toolbox.[17, 18] Furthermore, the droplet format is compatible with a wide range of molecular biology techniques and eliminates risks of cross-contamination.[2, 19–21]

However, droplet-microfluidics is limited in its capacity to perform true single-cell encapsulation, which impacts its ability to analyze precious samples of limited availability at the single-cell level. This is an important problem because clinical samples are usually available in low amount whether they are from needle biopsies, aspirates or washes. Single-cell analysis of such samples is significant as it can directly impact both our knowledge and treatment of cancer.[22–24] A high number of cells can be encapsulated at high-throughput using microfluidic droplet generators[25] but the cell distribution within droplets follows Poisson statistics, preventing an efficient single-cell encapsulation.[21, 26] To overcome this limitation, cells can be self-organized prior to their encapsulation using inertial effects.[27–29] Nevertheless, this approach requires very high flow rates and the volume range accessible is limited by the proximity to the jetting regime. Alternative strategies are based on the separation of droplets that contain single cells downstream of the droplet generator. Hydrodynamic sorting relies on size differences between empty and occupied droplets, thus yielding droplets with volumes dictated and limited by the size of the encapsulated cells.[30–32] Active droplet sorting is efficient but requires substantial off-chip equipment, labeled cells or active manipulation by an operator.[33–38]

To the best of our knowledge there is currently no passive platform that enables the single-cell analysis of rare samples, for which 100's to 1,000's of cells need to be encapsulated with a high success rate to minimize sample loss. Here, we report a novel method that relies on the trapping of single cells and their subsequent encapsulation in a single circuit. Our approach demonstrates an efficient and passive true single-cell encapsulation with minimal sample loss.

Strategy

Cells are first isolated and immobilized into individual traps, a series of which are used to create a linear array of hydrodynamic capturing sites.[39] Each trap consists of two flow paths, as depicted in Fig. 1a. The trapping pathway shortcuts the bypassing pathway via the trapping channel, a constricted conduit of sub-cellular dimensions. An incoming cell progresses through the unoccupied trapping pathway until it blocks the entrance of the trapping channel. The cell plugs that flow path (cell-plugging effect) and further flow is diverted through the bypass channel, effectively reconfiguring the local flow topology. We shortened the bypass channel to make the trapping and encapsulation steps compatible, and overcame the loss of trapping efficiency by incorporating structures that displace incoming cells towards the trapping pathway (displacement overhangs in Fig. 1a).

We harnessed the same cell-plugging principle to conduct single-cell encapsulation. Via this principle, the injected oil is diverted towards the bypass channel and thus surrounds the chamber containing a single-cell (Fig. 1b). Interestingly, this strategy yields two different modes of encapsulation: the bypass mode and the wetting-driven mode. Droplet generation is sequential and takes place at all occupied traps, resulting in true single-cell encapsulation.

The encapsulated cells can be recovered for further analysis by reversing the flow of oil (Fig. 1b). The three steps of our method (trapping, encapsulation and retrieval) are sequential, thus making the entire process fully deterministic.

Encapsulation modes

It is critical to fully understand the encapsulation processes to emphasize the constraints that informed the trapping strategy. Based on the oil injection rate and the surface properties of the chip, we could identify two successful modes of encapsulation. Both modes take advantage of the cell-plugging effect, but differ in the mechanisms leading to droplet generation. The captured cell plugs the trapping channel, thus diverting the incoming oil flow towards the bypass pathway. The oil first closes the chamber entry by forming an oil-water interface before progressing through the bypass channel. A droplet is not yet generated, but the aqueous flow is split: a small portion is stationary in the chamber, while the rest travels downstream the bypass channel.

In the bypass mode, the droplet is generated when the oil front progresses through the entire bypass channel and cuts off the side of the trapping channel opposite to the cell (Fig. 2a, SM1). Some secondary droplets are occasionally generated during the process but are rapidly evacuated by the flow of oil. The second mode of encapsulation is wetting-driven and encapsulation occurs when the oil wets the walls of the chamber and cuts off the trapping channel from within the chamber (Fig. 2b, SM2). This mode depends on a thin precursor film[40] that develops ahead of the macroscopic wetting front and creeps along the walls of the chamber until it reaches the trapping channel. The aqueous phase is thus surrounded by oil and a droplet is generated before the oil front can cut off the trapping channel from the bypass channel.

While both the bypass and wetting-driven modes result in the encapsulation of a single cell, their underlying principles are quite different. The wetting-driven mode depends on a series of quasi-equilibrium states, as a thin film of oil needs to develop along the chamber walls. This implies a very slow inflow of oil and an excellent oil wetting of the channel surfaces. On a practical level, the wetting-driven mode necessitates surface properties difficult to achieve reliably and provides limited throughput. Hence, we focused on the bypass mode, which is less dependent on surface properties and is relatively accommodating of various flow rates. Importantly, a captured cell can be extruded through the trapping channel if the pressure differential it experiences reaches a critical value (Fig. S1, SM3).[41] Thus, it would be necessary to design a short bypass channel with a large cross-section to minimize the pressure exerted on trapped cells when the oil flows through the bypass channel. However, these dimensional constraints have a detrimental impact on the cell trapping efficiency, necessitating the implementation of a counterbalancing strategy.

Trapping single cells with very high efficiency

A cell proceeds through the trapping pathway only if its center of mass is located within the streamlines that flow through the chamber.[42] As the incoming cells are distributed randomly across the cross-section of the channel, one can increase the probability of cell capture by

increasing the ratio of the flow through the trapping pathway over the flow through the bypassing channel (Q_{trap}/Q_{bypass}).[42, 43] It has been shown that a particle is preferentially directed towards a vacant trapping pathway if and only if $Q_{trap} > Q_{bypass}$.[39, 43–45] However, increasing the hydrodynamic resistance of the bypass channel by using a lengthy channel causes multiple problems: (1) cell clogging due to a limited shear rate through the bypassing pathway[46]; (2) high pressure differential exerted on the captured cells[47]; and (3) multiple particles per trap.[48] Importantly, a long bypass channel is not compatible with a reliable encapsulation as captured cells tend to be squeezed out due to an excessive pressure differential.

We adapted filtering structures[49] to focus cells towards the capturing streamlines and make single-cell capture compatible with the subsequent encapsulation (Fig. 3a). In our design, displacement overhangs coerce cells into crossing streamlines to ensure capture regardless of their initial position. The flow is locally split between the diverted flow going under the overhang (around 30% of the total flow in the configuration depicted here, Fig. S2), and the steering flow in the open channel section. The diverted flow is inaccessible to the typical cell, as the channel height below the overhangs is limited to 12 μm. Thus, a cell following a streamline heading under the overhang is displaced towards a steering flow streamline by sliding against the edge of the overhang. It is worth noting that a single overhang elicited a weaker displacement than the series of six structures used here (Fig. S3). This is supported by numerical simulations that show the generation of an elongated longitudinal vortex by repeated structures (Fig. 3b). Streamlines initially going below the overhangs (diverted flow) are steered towards the open channel section (steering flow) after passing underneath a couple of obstacles. Consequently, a series of overhangs leads to a better cell focusing. We studied the effect of the structures by reporting the lateral position of cells flowing through a straight channel comprising a series of overhangs (Fig. 3c–d). The normalized lateral position y is used to monitor the position of the cell (ESI). Plotting the final lateral position y_f as a function of the initial cell position y_i, shows that the overhangs efficiently displace cells (Fig. 3e). In our design, the series of overhangs is slanted compared to the walls of the channel to gradually increase the portion of flow going under the structures and minimize the number of constrictions with higher shear stress (Fig. 1a).

The complete plugging of the flow by a cell wedged into the trapping channel is essential to: (1) prevent the capture of multiple cells per trap, and (2) robustly conduct cell-plugging encapsulations. We engineered trapping channels with a square cross-section to ensure an efficient plugging of the flow by single-cells (Fig. 4a). This design assures that an efficient plugging can be achieved with cells of different size and stiffness, as demonstrated by our ability to use both live and fixed cells. It also reduces the likelihood of the cell being squeezed out through the trapping channel.[41, 48]

From the point of view of rare samples, it is critical to evaluate the percentage of cells that can be effectively trapped and thus further analyzed. Thus, we count the number of traps necessary to capture each cell to define the trapping efficiency. We injected A498 cancer cells (~ 10^5 cells/mL) using a syringe pump at low flow rate (6 to 20 μL/h) into a circuit primed with a 2% weight Pluronic F-68 solution in D-PBS. Cells are monitored as they progress through the hydrodynamic traps, and we recorded the trapping events at the first

vacant trap (Fig. 4b, SM4). Our data (n=566 cells) show that the incoming cell is captured by the first unoccupied trap in 93.8% of cases, and by the second empty trap 5.6% of the time (Fig. 4c). Interestingly, the trapping array is self-correcting because a cell not captured by the first site will be displaced towards the following trap by the flow going through the trapping channel left open. On very rare occasions (4 events, less than 0.6% of total number of cases), a cell is not trapped within the first two vacant traps but will statistically be trapped downstream given the trapping efficiency.

Cell capture is equally efficient for live and fixed cells. Aggregates of live cells are occasionally injected into the circuit, which result in multiple cells being trapped in a single capturing site. Nevertheless, a single cell is captured in more than 96% of the cases for live cells, while this rate reaches 99% for fixed cells.

By focusing incoming cells towards the trapping pathway, we fundamentally amend the $Q_{trap}>Q_{bypass}$ design rule and can reach a very high single-cell trapping efficiency using a short bypassing channel ($Q_{trap}/Q_{bypass} = 0.2$, Fig. S4) compatible with the encapsulation step. An incoming cell is highly likely (>99%) to be trapped within the next two empty traps, ensuring that any sample of live or fixed single-cells injected in our device can be reliably trapped without cell loss. Using those displacement structures, we effectively overcome the probabilistic nature of cell trapping[42] and obtained a near-perfect trapping efficiency.

Chip operation and droplet retrieval

To combine the single-cell trapping and encapsulation steps, we sequentially filled a tubing with fluorinated solution (2% weight PEG-based krytox surfactant[50] dissolved in HFE 7500) and a defined volume of cell solution (A498 cancer cells at 10^5 cells/mL). A498 cells exhibit a wide heterogeneity in size which ranges from 14 to 40 μm (Fig. S6). This approach prevents the presence of air bubbles and alleviates any troublesome tubing swapping during the transition between trapping and encapsulation. As the solution is injected and cells are captured, the oil interface progresses down the tubing until it reaches the circuit and seamlessly starts the encapsulation process.

Trapping and encapsulation are performed at the same flow rate: between 6 and 10 μl/h for live cells and 20 μl/h for fixed cells that can sustain higher flow rates without being squeezed through the trapping channels. We monitored all the encapsulation events as the oil progressed through the array of traps. An encapsulation event is considered a failure if no droplet is generated because the trapped cell is extruded through the trapping channel. The analysis of more than 2,000 events demonstrates that our platform dependably encapsulates live cells at a rate of 78% and fixed cells at a rate of 86% (Fig. 5a). Most failures are due to small deformable cells, which explains why fixed cells (which are stiffer) encapsulate at a higher rate. For live cells, we observed a size dependence of the extrusion process with cells smaller than 13 μm being extruded at a higher rate. For fixed cells, this bias towards smaller cells was not as clear. We obtained lower encapsulation rate (58%) with HeLa cells, which we attribute to their smaller size which ranges from 10 to 26 μm (Fig. S6). This lower success rate could be improved by using higher resolution lithography that would permit to

create narrower trapping channels able to accommodate smaller cells. It is crucial to note that no empty droplets are generated whether for live or fixed cells (Figs. S1 and S5).

The distributions of droplet volume for both live and fixed cells are unimodal and left-skewed (Fig 5b). We found that most droplets follow a normal distribution: 90% of the droplets have a volume of 164±9 pL for live cells; 85% of the droplets fall within the 155±8 pL range for fixed cells. Both distributions are centered on the estimated volume of the chamber (160 pL). The smaller droplets result from a leaking flow through the trapping channel when cells do not efficiently plug the flow. This effect is also observed for very rigid particles such as strongly fixed cells or polystyrene beads (data not shown). Those droplets could be corrected by using a plug of buffer and perform a circuit wide volume rectification via temporary merging and splitting allowed by the hydrodynamic trap format.[51] Alternatively, a simple filtering module could be used to make sure that none of the smaller droplets are further processed. The droplet content reflects the cell distribution during the trapping step (Fig. 5c), and most droplets contain a single cell. Further optimizing the preparation of the cell solution could minimize the aggregation of live cells before trapping.

Theoretically, the pressure required to trap and encapsulate single cells should not adversely affect their survival. We estimated using laminar flow assumption and typical pressure drop approximation[52] that the pressure drop across a single unit is 44 Pa for a flow of 10 μl/h, or 8.8 kPa across the entire device. This value is well below the stress-inducing range of hydrostatic pressure for mammalian cells that is estimated at a few MPa.[53] Finally, direct analysis of cell survival during the encapsulation process shows that an additional 5–10% of the cells are being compromised compared to the control (Fig. S7). This effect is likely due to squeezing during plugging.

Once the encapsulation is completed, we can retrieve the single-cell containing droplets by reversing the flow of oil (Fig. 6). This is achieved by slowly reducing the flow of incoming oil, unplugging the oil tubing and connecting another oil tubing into the outlet. The oil flow rate is incrementally increased to 40 μl/h to displace the droplets out of the traps. The droplet closest to the outlet is dislodged first and sequentially triggers the displacement of the other droplets while traveling through the circuit. At the level of a single module, the presence of a droplet in the bypass channel increases its effective hydrodynamic resistance and thus slightly increases the pressure differential across the trapping chamber. This pressure imbalance is sufficient to dislodge the trapped droplet (Fig. 6a). We are thus able to sequentially retrieve single-cell containing droplets (Fig. 6b, SM5). The overhangs do not affect the retrieval process, and we did not observe any droplet splitting. It is critical to note that the efficacies of encapsulation and droplet retrieval steps are highly dependent on surface properties of the channels. The device could also be re-used to repeat the whole operation of single-cell encapsulation and retrieval (see procedure in ESI). The main challenge in running the device stems from the requirement to maintain a single aqueous-oil interface. This requires careful flow switching. The typical operation time for each step are: (1) circuit priming, 5 minutes; (2) cell trapping, 5–10 minutes (fixed or live cells); (3) cell encapsulation, 2 minutes; (4) droplet retrieval, 10 minutes. The total operation time is thus below 30 minutes.

Overall, single-cells are efficiently trapped (99 %) and encapsulated (78–86 %) within droplets whose volume is solely set by the dimensions of the chamber, and the droplets generated can be retrieved for further processing.

Conclusions

In this paper, we report a novel and robust method for trapping, encapsulating, and retrieving single cells using passive principles such as flow reconfiguration by cell plugging. Our original strategy uncovered two modes of encapsulation. We focused on the bypass mode where an oil flow bypasses and partitions a chamber containing a single-cell. This encapsulation imposes strict rules on the circuit's design that are antagonistic to the trapping efficiency. We resolved that issue by integrating focusing structures that ensures a near-perfect trapping of single-cells and their encapsulation. The volume of the droplets is solely set by the geometry of the circuit, and no empty droplet is generated. The operation is mostly independent of the size of the cells, and smaller cells could be accommodated with a narrower trapping channel obtained with higher resolution lithography. We also clearly demonstrated its operation with cells that exhibit a wide range in size. Finally, droplets can be retrieved for further processing. The efficiency of our method and its ability to process heterogeneous samples make it ideally suited to manipulate precious samples such as clinical biopsies.

The number of cells processed could be easily increased by using parallel circuits. Interestingly, using a trapping scheme rather than a flow-through approach allows us to observe single-cells before further handling. This feature will allow the easy integration of microscopy with downstream sample processing to provide a fully integrated multiparameter platform that will impact the analysis of tissues at single-cell resolution.

Supplementary Material

Refer to Web version on PubMed Central for supplementary material.

Acknowledgments

References

1. Biesecker LG, Spinner NB. Nature Reviews Genetics. 2013; 14:307–320.

2. Zeng Y, Novak R, Shuga J, Smith MT, Mathies RA. Anal Chem. 2010; 82:3183–3190. [PubMed: 20192178]

3. Altschuler SJ, Wu LF. Cell. 2010; 141:559–563. [PubMed: 20478246]

4. Baret J-C, Beck Y, Billas-Massobrio I, Moras D, Griffiths AD. Chem Biol. 2010; 17:528–536. [PubMed: 20534350]

5. Huebner A, Srisa-Art M, Holt D, Abell C, Hollfelder F, Edel J. Chemical communications. 2007:1218–1220. [PubMed: 17356761]

6. Konry T, Dominguez-Villar M, Baecher-Allan C, Hafler DA, Yarmush ML. Biosensors and Bioelectronics. 2011; 26:2707–2710. [PubMed: 20888750]

7. Lu Y, Chen JJ, Mu L, Xue Q, Wu Y, Wu P-H, Li J, Vortmeyer AO, Miller-Jensen K, Wirtz D. Anal Chem. 2013; 85:2548–2556. [PubMed: 23339603]

8. White AK, VanInsberghe M, Petriv OI, Hamidi M, Sikorski D, Marra MA, Piret J, Aparicio S, Hansen CL. Proc Natl Acad Sci U S A. 2011; 108:13999–14004. [PubMed: 21808033]

9. Lindstrom S, Andersson-Svahn H. Lab Chip. 2010; 10:3363–3372. [PubMed: 20967379]

10. Reece A, Xia B, Jiang Z, Noren B, McBride R, Oakey J. Current opinion in biotechnology. 2016; 40:90–96. [PubMed: 27032065]

11. Wen N, Zhao Z, Fan B, Chen D, Men D, Wang J, Chen J. Molecules. 2016; 21

12. Pollen AA, Nowakowski TJ, Shuga J, Wang X, Leyrat AA, Lui JH, Li N, Szpankowski L, Fowler B, Chen P. Nature biotechnology. 2014; 32:1053–1058.

13. Zilionis R, Nainys J, Veres A, Savova V, Zemmour D, Klein AM, Mazutis L. Nature Protocols. 2017; 12:44–73. [PubMed: 27929523]

14. Klein AM, Mazutis L, Akartuna I, Tallapragada N, Veres A, Li V, Peshkin L, Weitz DA, Kirschner MW. Cell. 2015; 161:1187–1201. [PubMed: 26000487]

15. Akbari S, Pirbodaghi T. Lab Chip. 2014; 14:3275–3280. [PubMed: 24989431]

16. Joensson HN, Samuels ML, Brouzes ER, Medkova M, Uhlen M, Link DR, Andersson-Svahn H. Angew Chem Int Ed Engl. 2009; 48:2518–2521. [PubMed: 19235824]

17. Brouzes E, Medkova M, Savenelli N, Marran D, Twardowski M, Hutchison JB, Rothberg JM, Link DR, Perrimon N, Samuels ML. P Natl Acad Sci USA. 2009; 106:14195–14200.

18. Abate AR, Hung T, Mary P, Agresti JJ, Weitz DA. Proc Natl Acad Sci U S A. 2010; 107:19163–19166. [PubMed: 20962271]

19. He MY, Edgar JS, Jeffries GDM, Lorenz RM, Shelby JP, Chiu DT. Anal Chem. 2005; 77:1539–1544. [PubMed: 15762555]

20. Kumaresan P, Yang CJ, Cronier SA, Blazej RG, Mathies RA. Anal Chem. 2008; 80:3522–3529. [PubMed: 18410131]

21. Clausell-Tormos J, Lieber D, Baret JC, El-Harrak A, Miller OJ, Frenz L, Blouwolff J, Humphry KJ, Koster S, Duan H, Holtze C, Weitz DA, Griffiths AD, Merten CA. Chem Biol. 2008; 15:427–437. [PubMed: 18482695]

22. Navin N, Hicks J. Genome medicine. 2011; 3:31. [PubMed: 21631906]

23. Navin N, Kendall J, Troge J, Andrews P, Rodgers L, McIndoo J, Cook K, Stepansky A, Levy D, Esposito D, Muthuswamy L, Krasnitz A, McCombie WR, Hicks J, Wigler M. Nature. 2011; 472:90–94. [PubMed: 21399628]

24. Wang Y, Waters J, Leung ML, Unruh A, Roh W, Shi X, Chen K, Scheet P, Vattathil S, Liang H, Multani A, Zhang H, Zhao R, Michor F, Meric-Bernstam F, Navin NE. Nature. 2014; 512:155–160. [PubMed: 25079324]

25. Tan Y-C, Hettiarachchi K, Siu M, Pan Y-R, Lee AP. Journal of the American Chemical Society. 2006; 128:5656–5658. [PubMed: 16637631]

26. Koster S, Angile FE, Duan H, Agresti JJ, Wintner A, Schmitz C, Rowat AC, Merten CA, Pisignano D, Griffiths AD, Weitz DA. Lab Chip. 2008; 8:1110–1115. [PubMed: 18584086]

27. Edd JF, Di Carlo D, Humphry KJ, Koster S, Irimia D, Weitz DA, Toner M. Lab Chip. 2008; 8:1262–1264. [PubMed: 18651066]

28. Kemna EWM, Schoeman RM, Wolbers F, Vermes I, Weitz DA, van den Berg A. Lab Chip. 2012; 12:2881–2887. [PubMed: 22688131]

29. Schoeman RM, Kemna EWM, Wolbers F, van den Berg A. Electrophoresis. 2014; 35:385–392. [PubMed: 23856757]

30. Jing TY, Ramji R, Warkiani ME, Han J, Lim CT, Chen CH. Biosens Bioelectron. 2015; 66:19–23. [PubMed: 25460876]

31. Chabert M, Viovy JL. P Natl Acad Sci USA. 2008; 105:3191–3196.

32. Um E, Lee S-G, Park J-K. Applied Physics Letters. 2010; 97:153703.

33. Baret JC, Miller OJ, Taly V, Ryckelynck M, El-Harrak A, Frenz L, Rick C, Samuels ML, Hutchison JB, Agresti JJ, Link DR, Weitz DA, Griffiths AD. Lab Chip. 2009; 9:1850–1858. [PubMed: 19532959]

34. Agresti JJ, Antipov E, Abate AR, Ahn K, Rowat AC, Baret JC, Marquez M, Klibanov AM, Griffiths AD, Weitz DA. P Natl Acad Sci USA. 2010; 107:6550–6550.

35. Schmid L, Weitz DA, Franke T. Lab Chip. 2014; 14:3710–3718. [PubMed: 25031157]

36. Jang S, Lee B, Jeong H-H, Jin SH, Jang S, Kim SG, Jung GY, Lee C-S. Lab Chip. 2016; 16:1909–1916. [PubMed: 27102263]

37. Jin SH, Jeong H-H, Lee B, Lee SS, Lee C-S. Lab Chip. 2015; 15:3677–3686. [PubMed: 26247820]

38. Leung K, Zahn H, Leaver T, Konwar KM, Hanson NW, Page AP, Lo CC, Chain PS, Hallam SJ, Hansen CL. Proc Natl Acad Sci U S A. 2012; 109:7665–7670. [PubMed: 22547789]

39. Tan WH, Takeuchi S. Proc Natl Acad Sci U S A. 2007; 104:1146–1151. [PubMed: 17227861]

40. Bonn D, Eggers J, Indekeu J, Meunier J, Rolley E. Reviews of Modern Physics. 2009; 81:739–805.

41. Zhang Z, Xu J, Hong B, Chen X. Lab Chip. 2014; 14:2576–2584. [PubMed: 24895079]

42. Guan A, Shenoy A, Smith R, Li Z. Biomicrofluidics. 2015; 9:024103. [PubMed: 25825618]

43. Kobel S, Valero A, Latt J, Renaud P, Lutolf M. Lab Chip. 2010; 10:857–863. [PubMed: 20300672]

44. Kim H, Lee S, Lee JH, Kim J. Lab Chip. 2015; 15:4128–4132. [PubMed: 26369616]

45. Frimat JP, Becker M, Chiang YY, Marggraf U, Janasek D, Hengstler JG, Franzke J, West J. Lab Chip. 2011; 11:231–237. [PubMed: 20978708]

46. Chen YC, Allen SG, Ingram PN, Buckanovich R, Merajver SD, Yoon E. Sci Rep-Uk. 2015; 5

47. Chung KH, Rivet CA, Kemp ML, Lu H. Anal Chem. 2011; 83:7044–7052. [PubMed: 21809821]

48. Jin D, Deng B, Li JX, Cai W, Tu L, Chen J, Wu Q, Wang WH. Biomicrofluidics. 2015; 9

49. Choi S, Park JK. Lab Chip. 2007; 7:890–897. [PubMed: 17594009]

50. Holtze C, Rowat A, Agresti J, Hutchison J, Angile F, Schmitz C, Köster S, Duan H, Humphry K, Scanga R. Lab Chip. 2008; 8:1632–1639. [PubMed: 18813384]

51. Bithi SS, Wang WS, Sun M, Blawzdziewicz J, Vanapalli SA. Biomicrofluidics. 2014; 8:034118. [PubMed: 25379078]

52. Frenz L, Blank K, Brouzes E, Griffiths AD. Lab Chip. 2009; 9:1344–1348. [PubMed: 19417899]

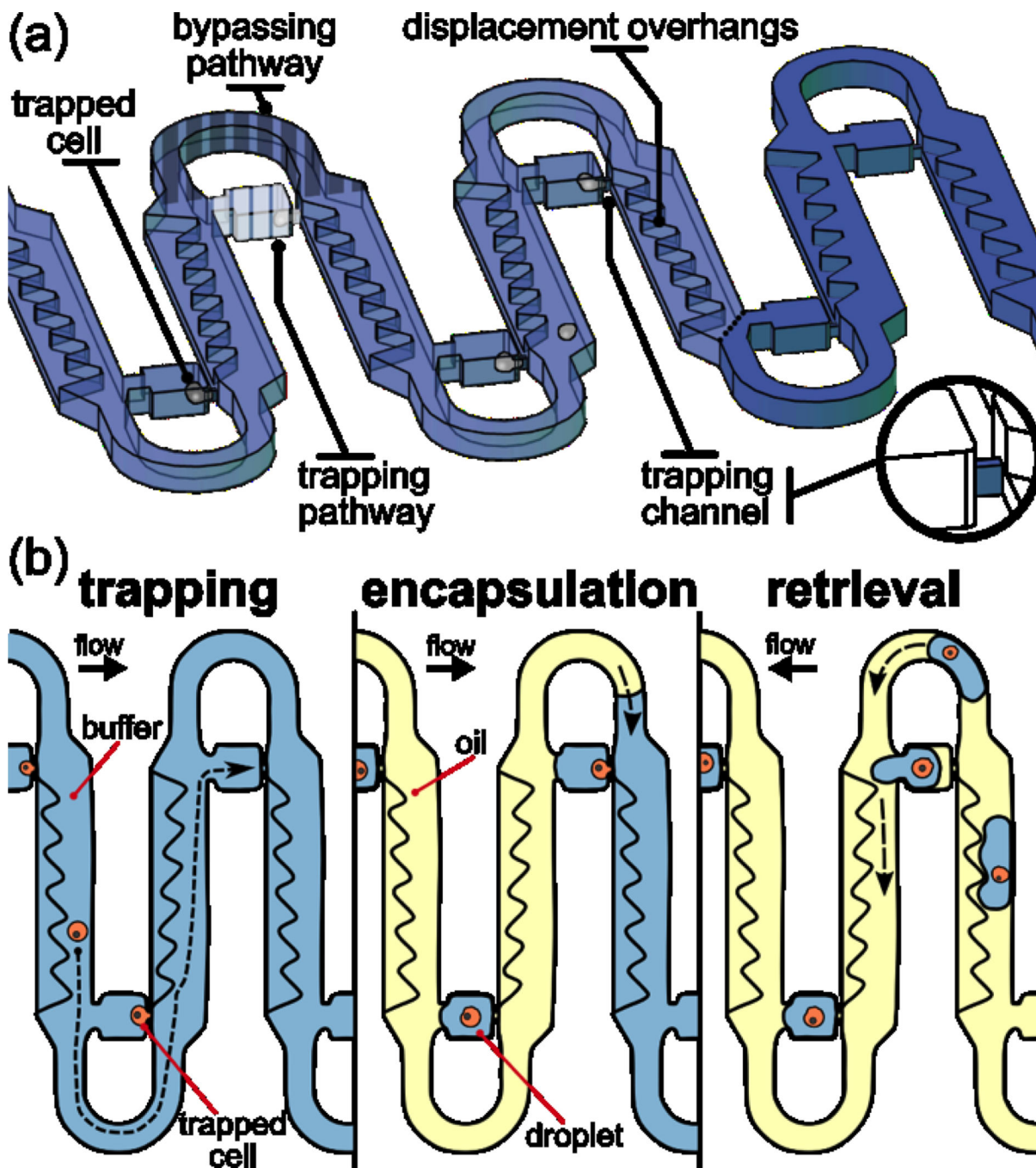53. Wang JH, Thampatty BP. Biomechanics and modeling in mechanobiology. 2006; 5:1–16. [PubMed: 16489478]

Fig. 1.
Schematics of the microfluidic circuit (a) and work flow (b) for true single-cell
encapsulation. Incoming cells are displaced towards the unoccupied trapping pathway by
focusing structures (displacement overhangs). Trapped cells plug the trapping channels,
diverting the flow and additional cells through the bypass pathway. The oil phase
sequentially flows around occupied traps, generating monodisperse droplets containing
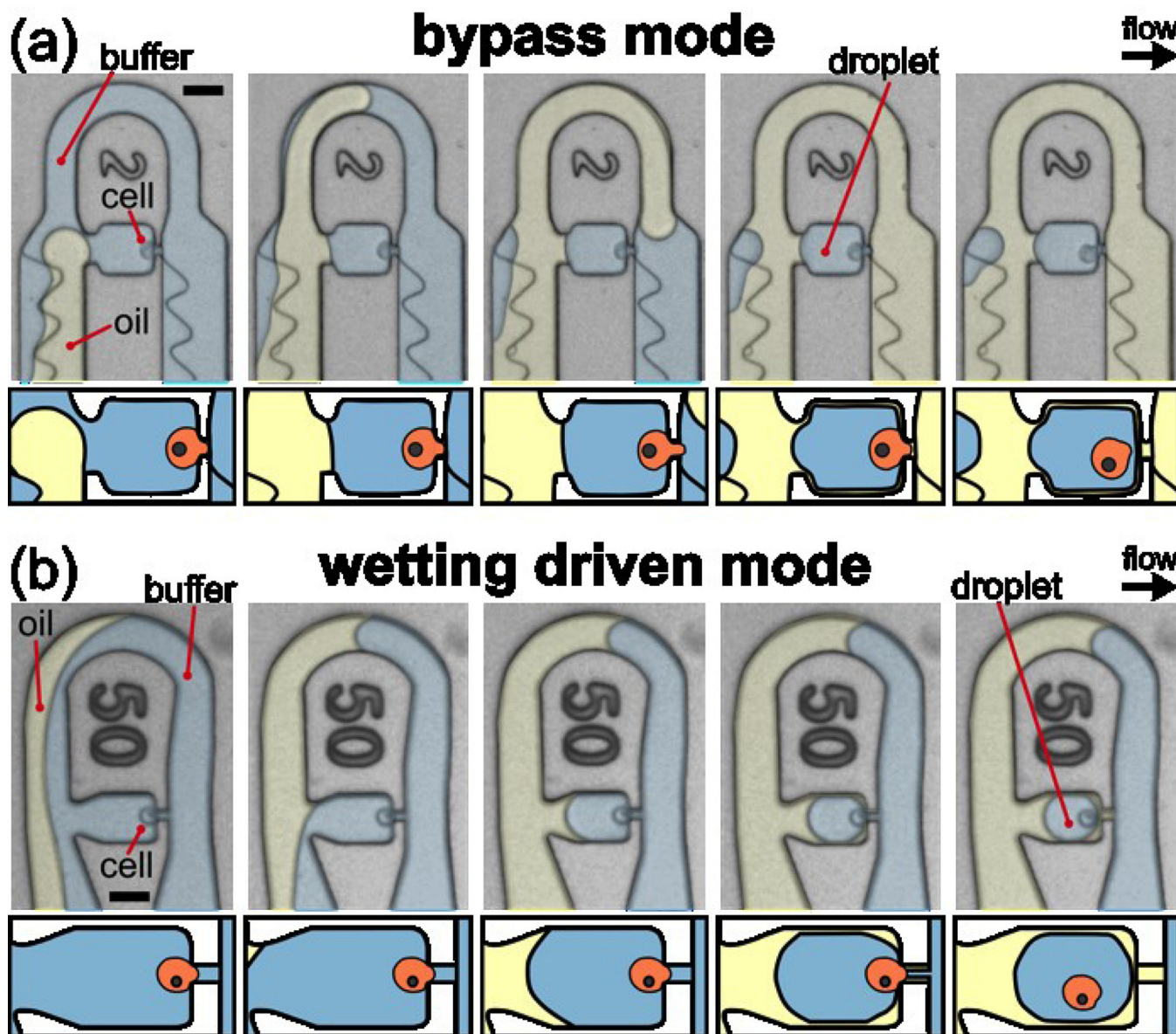single cells. The droplets are then retrieved by reversing the flow of oil.

Fig. 2.
Modes of encapsulation. (a) Bypass mode. The trapped cell blocks the flow through the trapping channel. The oil is diverted towards the bypassing pathway and finally surrounds the trapping chamber, generating a droplet containing a single-cell. (b) Wetting-driven mode is observed when the oil is injected at very low flow rates. A thin precursor film of oil wets ahead of the oil front, and progresses through the trapping channel until it cuts off the aqueous phase from within the chamber. Scale bars: 50 μm.
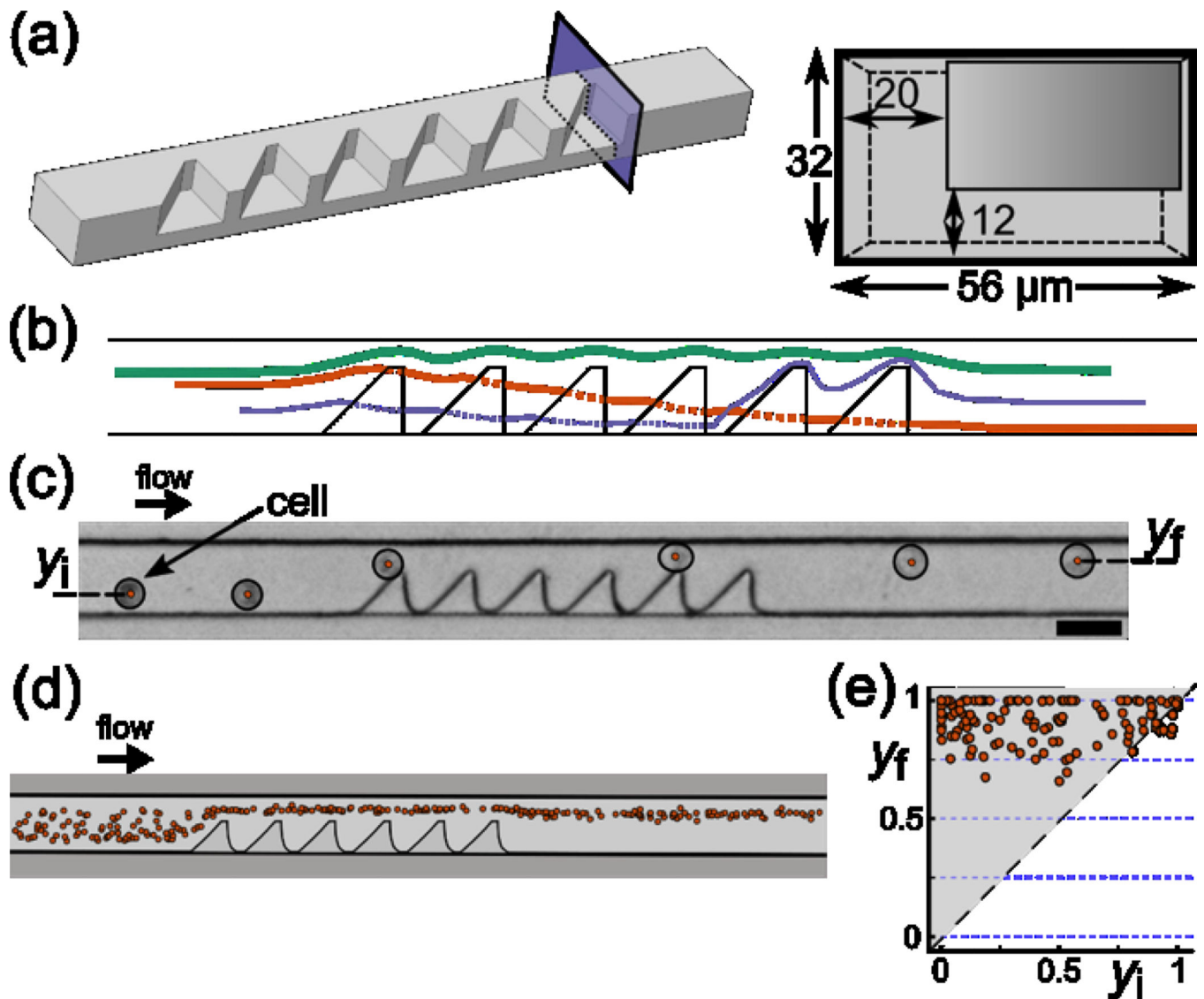
Fig. 3.
Impact of displacement structures. (a) 3D view and cross-section of the displacement structures. (b) Numerical simulations with COMSOL Multiphysics show that the order of streamlines is shifted by the overhang structures. (c) Time-lapse of a cell flowing through the structures shows how the centre of the cell is displaced from an initial position y_i, to a final position y_f. (d) The overlay of 37 cell trajectories emphasizes the impact of the displacement overhangs on the cell locations. (e) The plot of final positions vs initial positions (146 cells) clearly demonstrates the efficacy of cell displacement. Points on the diagonal would denote non-displaced cells, for instance in a channel without structures. Cells at the upper left of the graph were fully displaced from one side of the channel to the other.
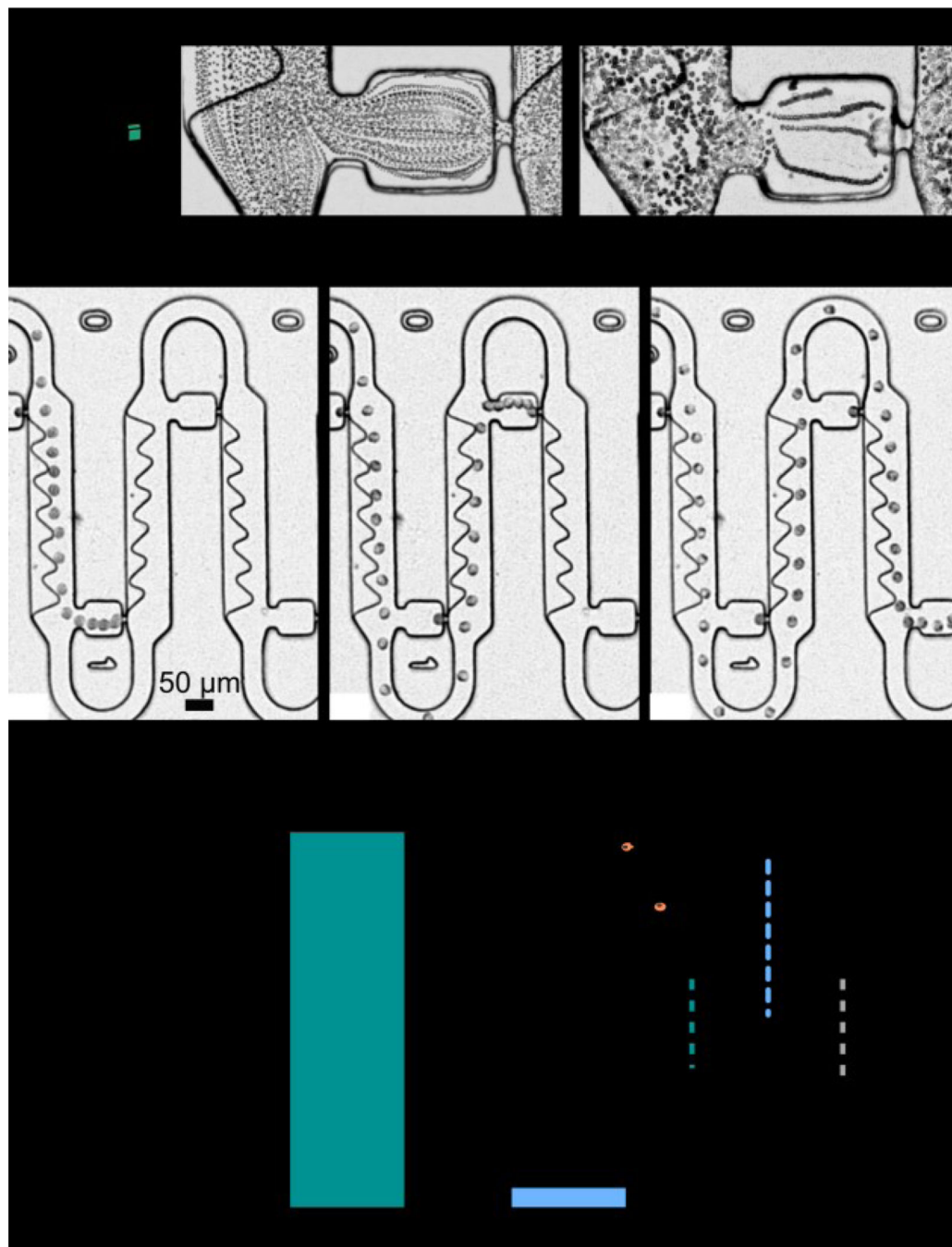
Fig. 4.
(a) Time lapse of seeded flow through a vacant and an occupied trap. The cell plugs the trapping channel and efficiently blocks the flow through the chamber. Scale bars: 50 μm. (b) Time-lapse of three cells trapped sequentially. Cells are coerced by the focusing structures, which optimizes cell capture. (c) Number of traps necessary to capture a cell. Single cells are mostly trapped by the next unoccupied trap (next), and the following one (next+1), with very few cells potentially not trapped by the array (>(next+1)).
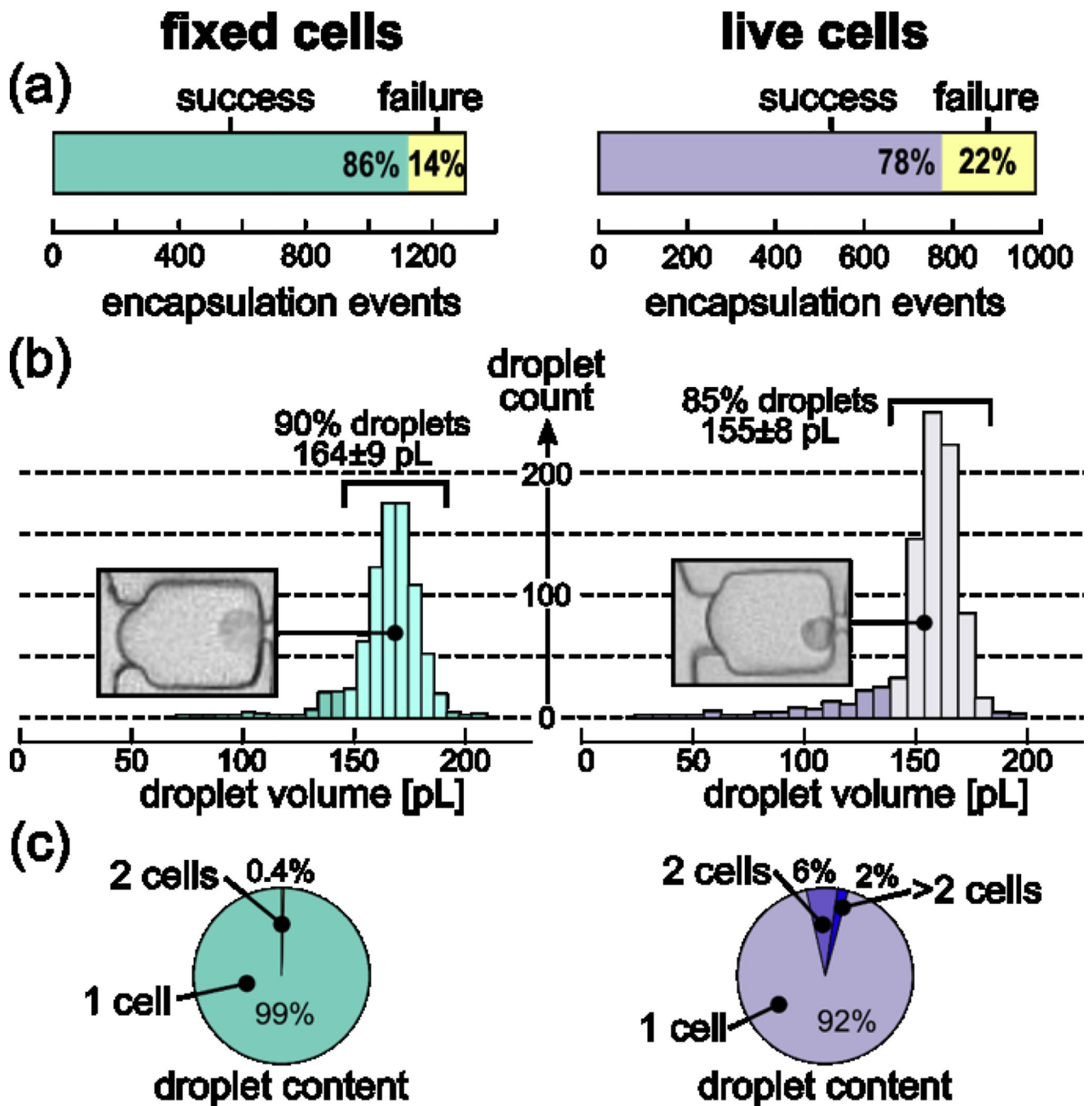
Fig. 5.
(a) Success rates of cell encapsulation. (b) Distribution of droplet volume for fixed and live cells. (c) Distribution of droplet content.
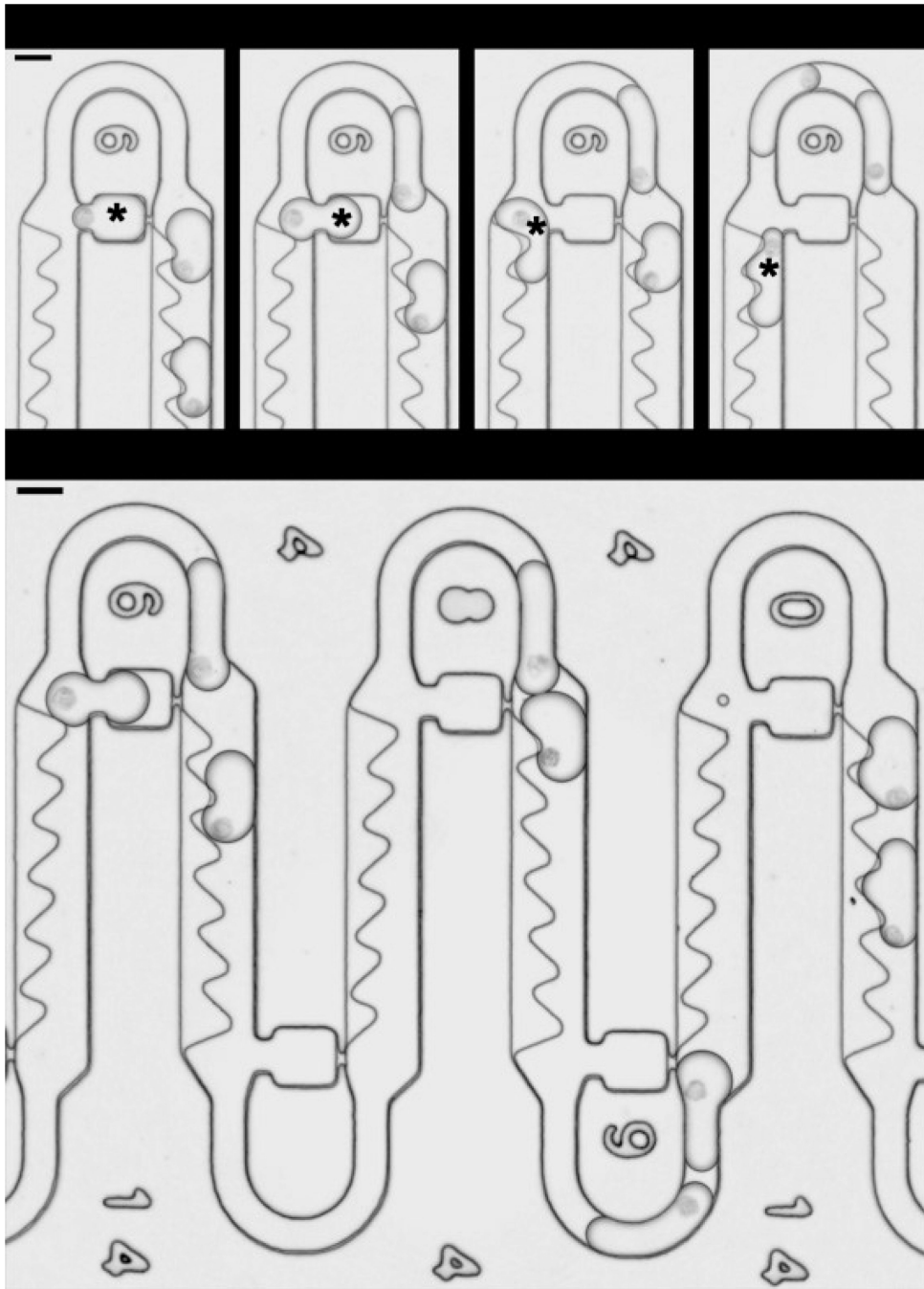
Fig. 6.
Droplet retrieval by reversing the flow of oil. (a) The incoming droplet dislodges the trapped droplet (marked by a star) when progressing through the bypass channel. (b) Overview of 9 dislodged droplets advancing through a circuit. Scale bars: 50 μm.